THE JOURNAL OF PHYSICAL CHEMISTRY Letters

Letter

pubs.acs.org/JPCL

Femtosecond Nanoplasmonic Dephasing of Individual Silver Nanoparticles and Small Clusters

Richa Mittal,[†] Rachel Glenn,[†] Ilyas Saytashev,[†] Vadim V. Lozovoy,[†] and Marcos Dantus*[,†,‡]

[†]Department of Chemistry, Michigan State University, 578 South Shaw Lane, East Lansing, Michigan 48824, United States

[‡]Department of Physics and Astronomy, Michigan State University, 567 Wilson Road, East Lansing, Michigan 48824, United States

W *Web-Enhanced Feature* *S* *Supporting Information*

ABSTRACT: We present experimental measurements of localized surface plasmon emission from individual silver nanoparticles and small clusters via accurately delayed femtosecond laser pulses. Fourier transform analysis of the nanoplasmonic coherence oscillations reveals different frequency components and dephasing rates for each nanoparticle. We find three different types of behavior: single exponential decay, beating between two frequencies, and beating among three or more frequencies. Our results provide insight into inhomogeneous and homogeneous broadening mechanisms in nanoplasmonic spectroscopy that depend on morphology and nearby neighbors. In addition, we find the optical response of certain pairs of nanoparticles to be at least an order of magnitude more intense than the response of single particles.

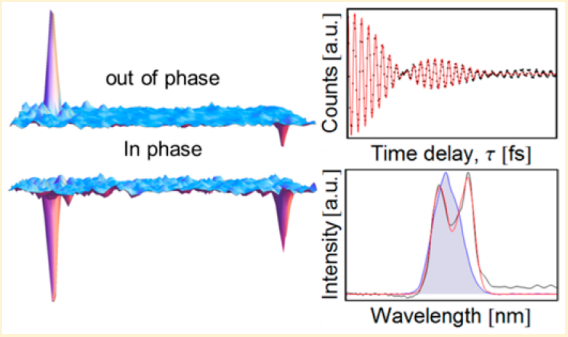

Nanoplasmonic emission arises from the collective localized response of the conduction electrons induced by an incident electric field.[1−3] Historically, the optical properties of plasmon active nanoparticles, such as their large optical cross sections and stability against photobleaching, made them useful for applications in stained glass windows. More importantly, under certain conditions, plasmon active surfaces have been found to give multiple-orders-of-magnitude enhancement of spectroscopic transitions, such as the well-known surface-enhanced Raman scattering (SERS).[4−7] This observation has led to a wide variety of applications such as biomedical imaging and sensing. The plasmonic response of individual nanoparticles and nanostructures depends on their shape, proximity to other nanoparticles, and coupling to the environment. Therefore, bulk spectroscopic measurements are obscured by significant heterogeneous broadening. Here we measure the linear localized surface plasmon polariton (LSP from here on) response of single and small clusters of silver nanoparticles to obtain their associated homogeneous dephasing time, a fundamental property related to the expected SERS.

Spectroscopic measurements of colloidal nanoparticles with narrow size distributions in solution and on substrates have led to the development of theories that describe how size, morphology, and interaction with the environment affect their resonant frequency and spectral shape.[8−15] Dephasing mechanisms such as radiative damping have been introduced to match experimentally measured spectral line shapes in simulation methods including discrete dipole approximation.[9] Studies combining optical and electron microscopy of individual nanoparticles have allowed a direct correlation between nanoparticle morphology and spectral line shape.[16−20] From dark-field microscopy and halogen lamp illumination measurements on 80 nm individual nanoparticles, dephasing times as short as 2 to 3 fs were inferred from the spectral line width.[17] Notwithstanding the progress that has been made by frequency-resolved spectroscopy, inferring dephasing times from spectroscopic measurements can be misleading, and direct time-resolved approaches are preferred.

Efforts toward direct time-resolved measurements of nanoplasmonic dephasing times have traditionally involved nonlinear optical processes, for example, second and third harmonic generation (SHG and THG).[21−23] Dephasing times as short as 7−10 fs have been measured by detecting the resulting SHG (at 400 nm) from an array of ∼200 nm silver nanoparticles. The measured times were twice as long as predicted by theory, partially because heterogeneous broadening had been mitigated through the lithographic creation of an array of identical nanoparticles. A lifetime of 6 fs was measured by detecting the THG (at 258 nm) from gold nanodisks (14 nm × 110−180 nm diameter). The amplitude and phase of the optical response from individual lithographically prepared silver nanoantena was recently measured.[24] The spectral amplitude showed a narrow resonance at 830 nm with a shoulder extending to bluer wavelengths within the bandwidth of the laser. Spectral hole-burning measurements with a tunable laser on elliptical silver nanoparticles found that the dephasing time depends on the incident photon energy (∼15 fs for 1.54 eV and ∼6 fs for 2.9 eV).[25,26] From two-

Received: February 7, 2015
Accepted: April 8, 2015

DOI: 10.1021/acs.jpclett.5b00264
J. Phys. Chem. Lett. 2015, 6, 1638−1644

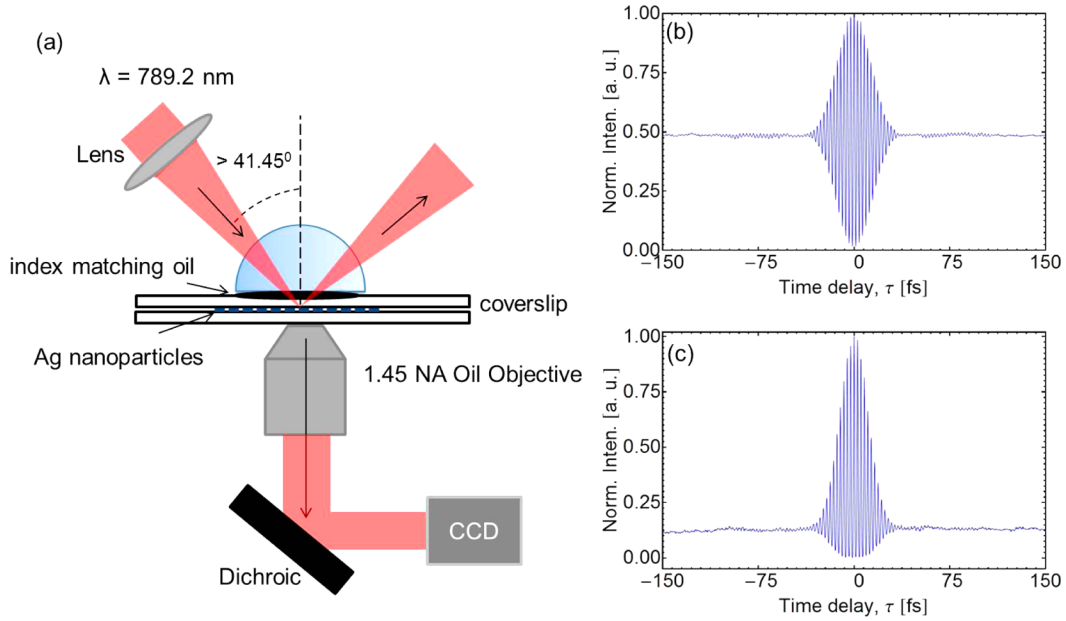

Figure 1. (a) Experimental wide-field total internal reflection microscopy setup. (b,c) Interferometric time delay scans of the 15.5 fs transform limited pulses for (b) the excitation pulse and (c) two-photon fluorescence emitted from polystyrene beads. The intensity plots are normalized at zero time delay.

photon autocorrelation measurements on a single ~75 nm silver nanoparticle using an 800 nm laser, a dephasing time of 10 fs was obtained.[27] Time-resolved two-photon electron photoemission from 2.2 nm silver nanoparticles deposited on graphite had a dephasing time of ~22 fs, with an intermediate state energy of 1.55 eV.[28] Two-photon photoemission measurements at 400 nm on silver gratings, with and without a propagating surface plasmon mode, detected a dephasing time of 4.9 to 5.8 fs.[29,30]

Conceptually, our linear dephasing-time measurements involve a femtosecond pulse with field $E(t)$ that induces a LSP, which emits coherent light proportional to the polarization $P(t)$.[23,28,30] A second pulse with delay τ induces an LSP within the same nanoparticle with emission proportional to $P(t - \tau)$. The detected signal $S(\tau)$ corresponds to the intensity of the field, which is proportional to the sum of the two polarizations as a function of time delay, $S(\tau) \approx \int |P^{(1)}(t) + P^{(1)}(t - \tau)|^2 \, dt$.[31,32] Initially the pulses overlap in time and one expects constructive and destructive interference at the carrier frequency of the laser. At later times, the measurement is sensitive to the longer lived plasmon resonance(s). The Fourier transform (FT) of the time-resolved signal yields the spectrum of the coherent emission $S(\omega) = \int S(\tau) e^{i\omega\tau} \, d\tau$. The spectrum $S(\omega)$ can be expressed as $S(\omega) = |P^{(1)}(\omega)|^2$,[31,32] where $P^{(1)}(\omega)$ is the FT of the polarization, $P^{(1)}(\omega) = \chi^{(1)}(\omega) \, E(\omega)$. The linear susceptibility $\chi^{(1)}(\omega)$ is given by

$$\chi^{(1)}(\omega) = \sum_{n}^{N} \alpha_n \frac{\gamma_n}{\omega - \omega_n + i\gamma_n} \tag{1}$$

where, for generality, we consider a number (N) of resonant frequencies with amplitude, α_n, resonance frequency, ω_n, and line width, γ_n. The spectral response function of the LSP $P^{(1)}(\omega)$ can be extracted using the definition of $S(\omega)$; this response function contains information about LSP frequencies and dephasing rates for each particle according to its size, shape, and surroundings.

The femtosecond dynamics of individual nanoparticles were measured using total internal reflection illumination and detected using a microscope objective, as shown in Figure 1. The measurements were carried out under wide-field illumination on tens of individual particles at the same time. The laser pulses (15.5 fs, at 800 nm with a Gaussian spectrum) (Figure 1b,c) were compressed by a pulse shaper, which also served to create the two pulse replica. (For detailed information, see the Experimental Methods.) The LSP emission from individual diffraction-limited bright spots was recorded as a function of the delay. Later, the sample was imaged using a scanning electron microscope (SEM), which allowed us to correlate the diffraction limited bright spots to single, double, or triple nanoparticle clusters.

Experimental results are shown in Figure 2. The left column shows time-domain plasmon-scattered signals from different silver nanoparticles and small clusters (see SEM insets). The original time scans spanned from −180 to 180 fs with a 0.25 fs time step (black dots) and were repeated three times. Given the symmetry gained by using two identical pulses, the positive and negative signals were averaged. The asymptote of the signal was set to zero based on the nature of a first-order signal, as previously discussed. The right column shows the data transformed into the frequency domain. This includes the experimental laser spectrum (shaded in blue), the Fourier transform of the experimental data using a 354 fs Hann window (black), and the fit based on the model $S(\omega)$, as previously described (red). The red curves in the time-domain plots are the inverse FT of the fit function in the frequency domain. Overall, single particles yield a LSP emission intensity that is lower (<200 counts), while the intensity of LSP emission from double and triple particles shows higher counts (~300 to over ~3000 counts).

For the single nanoparticles, we observed two types of behaviors. First, Figure 2a shows a modulated oscillating exponential. The FT of the time-resolved signal, shown in Figure 2f, reveals a narrow spectral band near 830 nm and a

DOI: 10.1021/acs.jpclett.5b00264
J. Phys. Chem. Lett. 2015, 6, 1638−1644

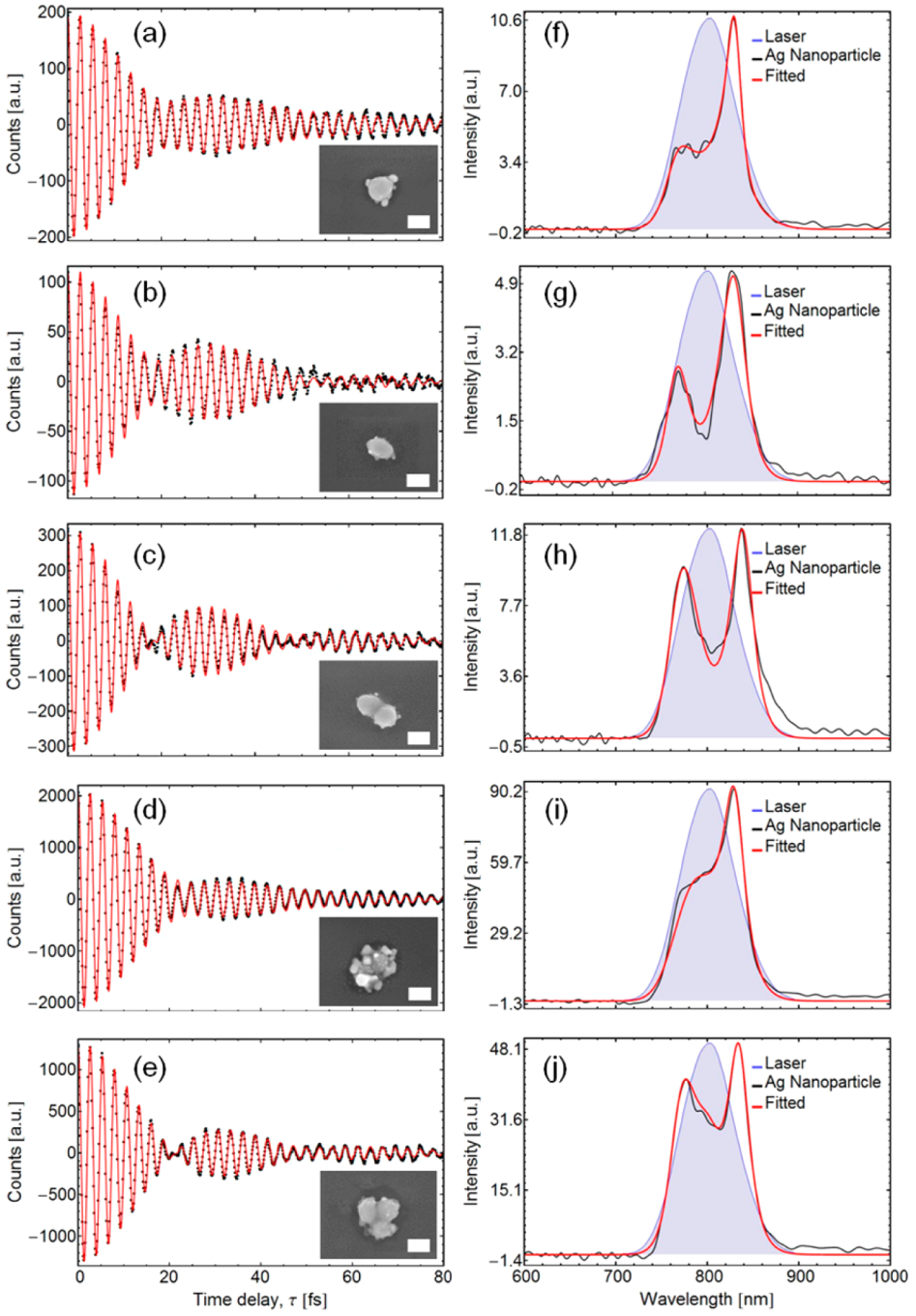

Figure 2. Plasmonic response of silver nanoparticles in the (a–e) time domain and (f–j) frequency domain for two singles, two pairs, and a small cluster of three nanoparticles. The insets show SEM images of the respective nanoparticles. Shown with the frequency domain is the FT (black), the fit (red), and the laser spectrum (shaded in blue). The scale bar is 100 nm long in all the SEM images, the nanoparticles are smooth, sub-50 nm features are an artifact from the osmium coating (see TEM images in the Supporting Information Figure S4).

broader spectral shoulder. The long-lived oscillations correspond to the narrow frequency, which in this case has a 28 ± 1 fs dephasing time T_2 deduced from the line width ($T_2 = 1/\gamma_n$ in eq 1). Second, we also see single-particle signals such as Figure 2b, where there is a more prominent second feature at ∼770 nm, as seen in Figure 2g. The SEM picture of the nanoparticle reveals an elliptical shape. We include two representative signals from pairs of nanoparticles in Figure 2c,d. Note that the signal is almost an order of magnitude greater for the latter particles. Also note that the colloidal particles used are smooth and quite regular in size (see TEM images in Figure S4 in the SI); any smaller features observed in the SEM pictures are artifacts resulting from the osmium coating and were caused during the image acquisition. Finally, we show the signal for a small cluster with three nanoparticles (Figure 2 e,j). Analysis of this data reveals three frequencies that span almost the entire laser spectrum.

Statistical analysis provides an overview of the different frequency components and dephasing rates of the nanoparticles. Table 1 contains the mean dephasing time T_2 obtained from the fitted line width for the individual resonances and their mean center wavelength. We find that longer

DOI: 10.1021/acs.jpclett.5b00264
J. Phys. Chem. Lett. 2015, 6, 1638–1644

Table 1. Mean Dephasing Time and Center Wavelength for the Different Resonances Obtained Following Spectral Fitting[a]

nanoparticles	dephasing time T_2 (fs)	wavelength (nm)
32 single	11 ± 5	771 ± 15
	28 ± 9	831 ± 4
10 double	8 ± 3	765 ± 15
	26 ± 4	831 ± 4
3 triple	11 ± 5	765 ± 15
	11 ± 5	800 ± 6
	27 ± 4	833 ± 4

[a]The dephasing time corresponds to ($T_2 = 1/\gamma_n$) values; the uncertainty quoted is $\pm\sigma$.

wavelength resonances have much longer dephasing times, as confirmed directly in the time-resolved data and by the presence of a sharp resonance in the frequency domain.

Measurements on single nanoparticles allow us to monitor their independent ultrafast dynamics. For example, in Figure 3, we show a pair of nanoparticles, where due to their frequency differences, their LSPR coherence is observed to be in phase at τ = 0, 38, and 75 fs and out of phase at τ = 22 and 54 fs. This behavior is illustrated in Figure 3 and in Multimedia 1.

We find that single round particles exhibit a narrow LSP resonance near 830 nm, with a smaller and broader shoulder near 770 nm. During the first ~20 fs, the time-resolved data are dominated by the interference between the pulses at 800 nm. It is also during early time delays that interaction between the nanoparticle and the substrate may be contributing to the signal.[10,26] Once the temporal overlap between the pulses is sufficiently small, red-shifting occurs due to electrodynamic retardation effects leading to the longer-lived plasmon resonance near 830 nm. This spectral shift is easier to appreciate by examining the spectrograms shown in Figure 4a,b, for which a 48 fs Hann window was scanned in time. The

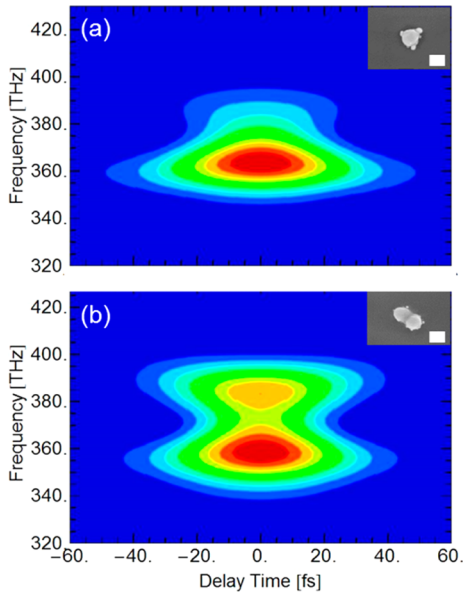

Figure 4. Time and frequency spectrograms obtained from the experimental data using a Hann window (fwhm 48 fs) scanned as a function of delay time. (a) Results from a single nanoparticle (corresponding to Figure 2a), and (b) results for a pair of nanoparticles (corresponding to Figure 2c).

Fourier transform (absolute value squared) at each time delay is performed to generate the contour plot. The resulting plots allow one to see the evolution of the signal as a function of time. Pairs of nanoparticles as well as small clusters give rise to two or more plasmon frequencies. The coupling between the particles gives rise to a blue- and a red-shifted emission.[1,25] The amplitude of the plasmonic response depends on the orientation of the pair of particles relative to the polarization of electric field and the distance (gap) between them.[33,34] The

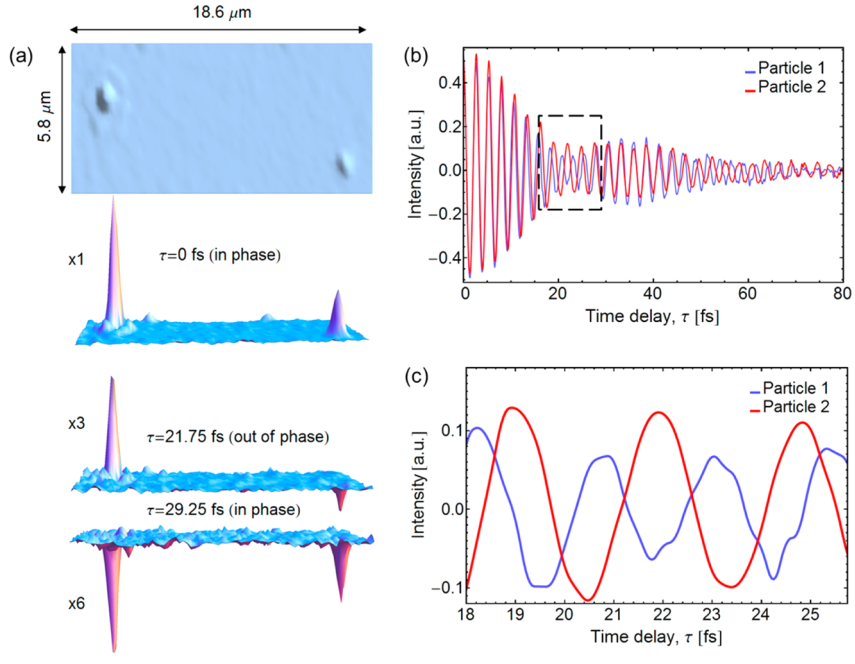

Figure 3. (a) 3D intensity plot of two particles (1, 2) at time delays: τ = 0 fs, 21.75 and 29.5 fs. Signal from both particles is enhanced by 3 times at τ = 21.75 fs and 6 times at τ = 29.5 fs to compensate the signal as it decays. (b) Comparison of the plasmon signal from the two nanoparticles, going in and out of phase as a function of time delay. (c) Zoom-in signal from τ = 18 to 26 fs time delays.

DOI: 10.1021/acs.jpclett.5b00264
J. Phys. Chem. Lett. 2015, 6, 1638−1644

influence of interparticle spacing has mostly been measured in 2D arrays of nanoparticles with various shapes and sizes.[35−37] The spectrogram shown in Figure 4b shows the emission from a pair of nanoparticles that contains two plasmon frequencies that are present after the laser pulses are no longer overlapped. Elliptical particles, as shown in Figure 2b, may also exhibit beating between two resonances at 830 and 770 nm; the frequencies depend on the ratio of the length of the two main axes.[25]

The measurements presented here provide direct measurement of the coherence dephasing for individual silver nanoparticles and small nanoparticle clusters. Our findings, obtained following off-resonance excitation of single nanoparticles, reflect a relatively long dephasing time of 28 ± 9 fs when exciting at 1.55 eV, with a red-shifted long-lived plasmon frequency at 1.49 eV. This value can be compared with the ∼15 fs dephasing time determined by spectral hole-burning at the same photon energy.[25,26] Dephasing measurements following direct excitation at 3.01 eV or following two 1.55 eV two-photon excitations have yielded ∼10 and ∼22 fs for 75 and 2.2 nm particles, respectively.[27,28] The values reported here correspond to $T_2 = 1/\gamma_n$; it is possible that there may be a factor-of-two difference between our measurements and plasmon lifetime values in the literature. Note our time-resolved data and the width of the plasmon frequency are consistent with the ∼28 fs dephasing found for single particles. An additional reason for the relatively long dephasing times is that our experiments were carried out far from resonance. Dephasing times are expected to be longer at 1.55 eV because radiation damping is strongly frequency-dependent $\sim\omega^3$.[38] For pairs of nanoparticles and triple particle clusters we find that most of the intensity decays within the first ∼10 fs; however, we still see a long-lived ∼27 fs component at longer wavelengths, albeit with much lower intensity. In connection with SERS, we confirm that small clusters lead to a plasmonic response that overlaps the entire excitation spectrum, and thus it provides the highest peak intensity. The broader bandwidth is better suited to couple to molecular vibrational bonds. Dephasing mechanisms include electron−electron interactions, electron−surface scattering,[39] and radiative damping.[40,41] This implies that for high-quality colloidal nanoparticles excited at longer wavelengths a longer dephasing time is expected. Future experiments will explore dephasing mechanisms through comparison of smooth nanodisks to nanoprisms containing sharp corners. The information resulting from these types of direct time-resolved measurements should help refine theoretical models and may be relevant to applications for which silver nanoparticles play the role of nanoantennas, for example, in biosensing applications and even in solar energy capture.[42,43]

EXPERIMENTAL METHODS

The experimental setup consists of a femtosecond laser, pulse shaper, and a total internal reflection (TIR) microscope (Figure 1a) similar to the setup used by Stock et al.[44] The laser beam from a Ti:sapphire oscillator (KMLabs) producing pulses at 85 MHz centered at 800 and ∼64 nm bandwidth (fwhm) was guided to a phase-amplitude pulse shaper. The 4f pulse-shaper (MIIPS box 640, Biophotonic Solutions Inc.) utilizes a liquid-crystal spatial light modulator with 640 pixels at the Fourier plane. The output beam from the pulse shaper was directed to the sample plane using an adjustable mirror, focusing lens (focal length, f = 500 mm), and hemispheric prism. The adjustable mirror determined the TIR illumination angle such that $\theta > \theta_c$, the critical angle for total internal reflection. On the basis of the refractive index for BK7 glass and air at 800 nm, a critical angle θ_c of ∼41.5° was calculated. The signal emitted by TIR illumination was collected using a high NA objective (CFI Plan Apo TIRF 60×/1.45 NA oil, Nikon). The wide-field images were recorded by a thermoelectrically cooled electron multiplying CCD camera (iXon DV887, Andor). For in situ pulse characterization, two photon excited fluorescence from fluorescent beads and an additional band-pass (BP 550 nm) filter in the collection arm were used. The average power of the incident laser beam at the sample was ∼18 μW, and the beam was focused on the sample to a focal spot size of 100 μm, resulting in an energy fluence of ∼2.6 nJ/cm^2 and peak intensity of ∼1.9 × 10^5 W/cm^2.

The pulses were initially characterized and compressed at the focal plane of an alternate, but equivalent, optical arm using multiphoton intrapulse interference phase scan (MIIPS).[45,46] A Gaussian amplitude transmission window was used to obtain Gaussian pulses in the time domain. The dependence of two-photon excited fluorescence signal from fluorescent microspheres as a function of chirp was obtained to confirm the presence of transform-limited pulses at the focal plane of the microscope (Figure S1 in the SI). This ensured delivery of 15.5 fs transform-limited pulses. Interferometric time-delay scans were performed by creating identical pulses using the pulse shaper.[47] The linear optical interference between the fundamental excitation laser pulses (Figure 1b) and the in situ TPEF autocorrelation (Figure 1c) confirm the laser characteristics. Both the fundamental laser spectrum with and without a Gaussian mask are shown in Figure S2 in the SI. The interferometric autocorrelation of the laser is shown in Figure S3 in the SI.

The silver nanoparticles studied were purchased from Sigma-Aldrich (no. 730777). The sample was sonicated (∼2.5 h.) to ensure single isolated nanoparticles and placed on the glass slide and dried to be studied under the TIR microscope. After the time-resolved measurements were concluded, the sample was coated with a 10 nm of osmium and imaged by scanning electron microscope (SEM, inserts in Figure 2). The size distribution of the particles was determined by transmission electron microscopy (TEM, Figure S4 in the SI). The nominally round particles (Figure S4 in the SI) had an elliptical variation that can be described by a short axis dimension of average 85 ± 12 nm and a long axis dimension of 100 ± 15 nm. The ratio between the two axes varied between 6 and 26%. The linear absorption spectrum of the silver nanoparticles solution is shown in Figure S5 in the SI. All measurements were taken at room temperature under ambient conditions.

Each wide-field image contains tens of nanoparticles; diffraction-limited LSP signals are analyzed independently by averaging the raw counts within 5 × 5 bright pixels. The background from the immediately surrounding pixels is selected and subtracted. Finally, the long-time >150 fs asymptotic signal level is subtracted. Data from three independent measurements were averaged and then Fourier-transformed. To improve the FT results, a Hann window with fwhm 354 fs was applied at τ = 0 to the time-resolved signal for each nanoparticle. The dephasing times and resonances were extracted from the fitting function parameters in the frequency domain.

DOI: 10.1021/acs.jpclett.5b00264
J. Phys. Chem. Lett. 2015, 6, 1638−1644

■ ASSOCIATED CONTENT

Supporting Information

Confirmation that there was no residual chirp on the incident pulses at the focal plane. Laser spectrum before and after Gaussian spectral correction. Interferometric autocorrelation of the laser pulses obtained by two-photon excited fluorescence at the focal plane of the microscope confirming 15.5 fs pulse duration. TEM images of the nanoparticles as deposited. Extinction spectrum of the solution of colloidal silver nanoparticles used to prepare the samples. This material is available free of charge via the Internet at http://pubs.acs.org.

Web-Enhanced Feature

A movie of independent ultrafast dynamics of single nanoparticles in AVI format is available in the online version of the paper.

■ AUTHOR INFORMATION

Corresponding Author

*E-mail: dantus@msu.edu.

Notes

The authors declare no competing financial interest.

■ ACKNOWLEDGMENTS

We thank Mark I. Stockman for discussions concerning the dephasing rate for silver nanoparticles at 800 nm and suggestions for new experiments. We also thank George Schatz for illuminating discussions. Financial support of this work comes from the Chemical Sciences, Geosciences and Biosciences Division, Office of Basic Energy Sciences, Office of Science, U.S. Department of Energy, DOE SISGR (DE-SC0002325), Dr. Jeff Krause, Program Manager. R.M. acknowledges support from the Center of Research Excellence in Complex Materials (CORE-CM) at Michigan State University. We thank Elena Bongiovanni for her help in proofreading the manuscript.

■ REFERENCES

(1) Kelly, K. L.; Coronado, E.; Zhao, L. L.; Schatz, G. C. The Optical Properties of Metal Nanoparticles: The Influence of Size, Shape, and Dielectric Environment. *J. Phys. Chem. B* **2003**, *107*, 668−677.

(2) Bouhelier, A.; Beversluis, M. R.; Novotny, L. Characterization of Nanoplasmonic Structures by Locally Excited Photoluminescence. *Appl. Phys. Lett.* **2003**, *83*, 5041−5043.

(3) Stockman, M. I. Nanoplasmonics: Past, Present, and Glimpse into Future. *Opt. Express* **2011**, *19*, 22029−22106.

(4) Fleischmann, M.; Hendra, P. J.; McQuillan, A. J. Raman Spectra of Pyridine Adsorbed at a Silver Electrode. *Chem. Phys. Lett.* **1974**, *26*, 163−166.

(5) Jeanmaire, D. L.; Van Duyne, R. P. Surface Raman Spectroelectrochemistry: Part I. Heterocyclic, Aromatic, and Aliphatic Amines Adsorbed on the Anodized Silver Electrode. *J. Electroanal. Chem. Interfacial Electrochem.* **1977**, *84*, 1−20.

(6) Schultz, S. G.; Janik-Czachor, M.; Van Duyne, R. P. Surface Enhanced Raman Spectroscopy: A Re-Examination of the Role of Surface Roughness and Electrochemical Anodization. *Surf. Sci.* **1981**, *104*, 419−434.

(7) Willets, K. A.; Van Duyne, R. P. Localized Surface Plasmon Resonance Spectroscopy and Sensing. *Annu. Rev. Phys. Chem.* **2007**, *58*, 267−297.

(8) Jensen, T. R.; Schatz, G. C.; Van Duyne, R. P. Nanosphere Lithography: Surface Plasmon Resonance Spectrum of a Periodic Array of Silver Nanoparticles by Ultraviolet−Visible Extinction Spectroscopy and Electrodynamic Modeling. *J. Phys. Chem. B* **1999**, *103*, 2394−2401.

(9) Jensen, T.; Kelly, L.; Lazarides, A.; Schatz, G. C. Electrodynamics of Noble Metal Nanoparticles and Nanoparticle Clusters. *J. Cluster Sci.* **1999**, *10*, 295−317.

(10) Sherry, L. J.; Chang, S.-H.; Schatz, G. C.; Van Duyne, R. P.; Wiley, B. J.; Xia, Y. Localized Surface Plasmon Resonance Spectroscopy of Single Silver Nanocubes. *Nano Lett.* **2005**, *5*, 2034−2038.

(11) Aikens, C. M.; Li, S.; Schatz, G. C. From Discrete Electronic States to Plasmons: TDDFT Optical Absorption Properties of Agn (n = 10, 20, 35, 56, 84, 120) Tetrahedral Clusters. *J. Phys. Chem. C* **2008**, *112*.

(12) Draine, B. T.; Flatau, P. J. Discrete-Dipole Approximation for Periodic Targets: Theory and Tests. *J. Opt. Soc. Am. A* **2008**, *25*, 2693−2703.

(13) Weissker, H. C.; Mottet, C. Optical Properties of Pure and Core-Shell Noble-Metal Nanoclusters From TDDFT: The Influence of the Atomic Structure. *Phys. Rev. B* **2011**, *84*, 165443.

(14) Bae, G.-T.; Aikens, C. M. Time-Dependent Density Functional Theory Studies of Optical Properties of Ag Nanoparticles: Octahedra, Truncated Octahedra, and Icosahedra. *J. Phys. Chem. C* **2012**, *116*, 10356−10367.

(15) Crut, A.; Maioli, P.; Fatti, N. D.; Vallée, F. Optical Absorption and Scattering Spectroscopies of Single Nano-Objects. *Chem. Soc. Rev.* **2014**, *43*, 3921−3956.

(16) Mock, J. J.; Barbic, M.; Smith, D. R.; Schultz, D. A.; Schultz, S. Shape Effects in Plasmon Resonance of Individual Colloidal Silver Nanoparticles. *J. Chem. Phys.* **2002**, *116*, 6755−6759.

(17) Sönnichsen, C.; Franzl, T.; Wilk, T.; von Plessen, G.; Feldmann, J. Plasmon Resonances in Large Noble-Metal Clusters. *New J. Phys.* **2002**, *4*, 93.1−93.8.

(18) van Dijk, M. A.; Lippitz, M.; Orrit, M. Detection of Acoustic Oscillations of Single Gold Nanospheres by Time-Resolved Interferometry. *Phys. Rev. Lett.* **2005**, *95*, 267406.

(19) Muskens, O. L.; Del Fatti, N.; Vallée, F. Femtosecond Response of a Single Metal Nanoparticle. *Nano Lett.* **2006**, *6*, 552−556.

(20) van Dijk, M. A.; Lippitz, M.; Stolwijk, D.; Orrit, M. A Common-Path Interferometer for Time-Resolved and Shot-Noise-Limited Detection of Single Nanoparticles. *Opt. Express* **2007**, *15*, 2273−2287.

(21) Lamprecht, B.; Leitner, A.; Aussenegg, F. R. Femtosecond Decay-Time Measurement of Electron-Plasma Oscillation in Nanolithographically Designed Silver Particles. *Appl. Phys. B: Laser Opt.* **1997**, *64*, 269−272.

(22) Lamprecht, B.; Leitner, A.; Aussenegg, F. R. SHG Studies of Plasmon Dephasing in Nanoparticles. *Appl. Phys. B: Laser Opt.* **1999**, *68*, 419−423.

(23) Lamprecht, B.; Krenn, J. R.; Leitner, A.; Aussenegg, F. R. Resonant and Off-Resonant Light-Driven Plasmons in Metal Nanoparticles Studied by Femtosecond-Resolution Third-Harmonic Generation. *Phys. Rev. Lett.* **1999**, *83*, 4421−4424.

(24) Accanto, N.; Piatkowski, L.; Renger, J.; van Hulst, N. F. Capturing the Optical Phase Response of Nanoantennas by Coherent Second-Harmonic Microscopy. *Nano Lett.* **2014**, *14*, 4078−4082.

(25) Stietz, F.; Bosbach, J.; Wenzel, T.; Vartanyan, T.; Goldmann, A.; Träger, F. Decay Times of Surface Plasmon Excitation in Metal Nanoparticles by Persistent Spectral Hole Burning. *Phys. Rev. Lett.* **2000**, *84*, 5644−5647.

(26) Bosbach, J.; Hendrich, C.; Stietz, F.; Vartanyan, T.; Träger, F. Ultrafast Dephasing of Surface Plasmon Excitation in Silver Nanoparticles: Influence of Particle Size, Shape, and Chemical Surrounding. *Phys. Rev. Lett.* **2002**, *89*, 257404.

(27) Liau, Y.-H.; Unterreiner, A. N.; Chang, Q.; Scherer, N. F. Ultrafast Dephasing of Single Nanoparticles Studied by Two-Pulse Second-Order Interferometry. *J. Phys. Chem. B* **2001**, *105*, 2135−2142.

(28) Merschdorf, M.; Kennerknecht, C.; Pfeiffer, W. Collective and Single-Particle Dynamics in Time-Resolved Two-Photon Photoemission. *Phys. Rev. B* **2004**, *70*.

(29) Kubo, A.; Jung, Y. S.; Kim, H. K.; Petek, H. Femtosecond Microscopy of Localized and Propagating Surface Plasmons in Silver Gratings. *J. Phys. B* **2007**, *40*.

DOI: 10.1021/acs.jpclett.5b00264
J. Phys. Chem. Lett. 2015, 6, 1638−1644

(30) Bayer, D.; Wiemann, C.; Gaier, O.; Bauer, M.; Aeschlimann, M. Time-Resolved 2PPE and Time-Resolved PEEM as a Probe of LSP's in Silver Nanoparticles. *J. Nanomater.* **2008**, *2008*, 249514.
(31) Mukamel, S. *Principles of Nonlinear Optical Spectroscopy*; Oxford University Press: New York, 1999; p 576.
(32) Boyd, R. W. *Nonlinear Optics*, 3rd ed.; Academic Press: Boston, 2008; p 640.
(33) Zhao, K.; Troparevsky, M. C.; Xiao, D.; Eguiluz, A. G.; Zhang, Z. Electronic Coupling and Optimal Gap Size between Two Metal Nanoparticles. *Phys. Rev. Lett.* **2009**, *102*, 186804.
(34) Sheikholeslami, S.; Jun, Y.-w.; Jain, P. K.; Alivisatos, A. P. Coupling of Optical Resonances in a Compositionally Asymmetric Plasmonic Nanoparticle Dimer. *Nano Lett.* **2010**, *10*, 2655−2660.
(35) Haynes, C. L.; McFarland, A. D.; Zhao, L.; Van Duyne, R. P.; Schatz, G. C.; Gunnarsson, L.; Prikulis, J.; Kasemo, B.; Käll, M. Nanoparticle Optics: The Importance of Radiative Dipole Coupling in Two-Dimensional Nanoparticle Arrays. *J. Phys. Chem. B* **2003**, *107*, 7337−7342.
(36) Malynych, S.; Chumanov, G. Light-Induced Coherent Interactions between Silver Nanoparticles in Two-Dimensional Arrays. *J. Am. Chem. Soc.* **2003**, *125*, 2896−2898.
(37) Kinnan, M. K.; Chumanov, G. Plasmon Coupling in Two-Dimensional Arrays of Silver Nanoparticles: II. Effect of the Particle Size and Interparticle Distance. *J. Phys. Chem. C* **2010**, *114*, 7496−7501.
(38) Scharte, M.; Porath, R. Do Mie Plasmons have a Longer Lifetime on Resonance than Off Resonance? *Appl. Phys. B: Laser Opt.* **2001**, *73*, 305−310.
(39) Kreibig, U.; Vollmer, M. *Optical Properties of Metal Clusters*; Springer: New York, 1995.
(40) Wokaun, A.; Gordon, J. P.; Liao, P. F. Radiation Damping in Surface-Enhanced Raman Scattering. *Phys. Rev. Lett.* **1982**, *48*, 957−960.
(41) Vartanyan, T.; Simon, M. Femtosecond Optical Second Harmonic Generation by Metal Clusters: The Influence of Inhomogeneous Line Broadening on the Dephasing Time of Surface Plasmon Excitation. *Appl. Phys. B: Laser Opt.* **1999**, *68*, 425−431.
(42) Rosi, N. L.; Mirkin, C. A. Nanostructures in Biodiagnostics. *Chem. Rev.* **2005**, *105*, 1547−1562.
(43) Takai, A.; Kamat, P. V. Capture, Store, and Discharge. Shuttling Photogenerated Electrons Across TiO2-Silver Interface. *ACS Nano* **2011**, *5*, 7369−7376.
(44) Stock, K.; Sailer, R.; Strauss, W.; Lyttek, M.; Steiner, R.; Schneckenburger, H. Variable-Angle Total Internal Reflection Fluorescence Microscopy (VA-TIRFM): Realization and Application of a Compact Illumination Device. *J. Microsc.* **2003**, *211*, 19−29.
(45) Lozovoy, V. V.; Pastirk, I.; Dantus, M. Multiphoton Intrapulse Interference.IV.Ultrashort Laserpulse Spectral Phase Characterization and Compensation. *Opt. Lett.* **2004**, *29*, 775−777.
(46) Coello, Y.; Lozovoy, V. V.; Gunaratne, T. C.; Xu, B.; Borukhovich, I.; Tseng, C.-h.; Weinacht, T.; Dantus, M. Interference without an Interferometer: a Different Approach to Measuring, Compressing, and Shaping Ultrashort Laser Pulses. *J. Opt. Soc. Am. B* **2008**, *25*, A140−A150.
(47) Konar, A.; Lozovoy, V. V.; Dantus, M. Electronic Dephasing of Molecules in Solution Measured by Nonlinear Spectral Inteferometry. *ScienceJet* **2015**,, *4*, 141.

DOI: 10.1021/acs.jpclett.5b00264
J. Phys. Chem. Lett. 2015, 6, 1638−1644